Check for updates

ChemEurJ

Research Article
doi.org/10.1002/chem.202502835

Chemistry Europe
European Chemical Societies Publishing

www.chemeurj.org

Golgi-Targeted Viscosity Fluorescent Probe for Monitoring Acute Lung Injury

Yaqian Li,[a] Zi Yang,[a] Jieni Lei,[a] Qiuzi Dai,[a] Guangyi Li,[a] Hai Xu,*[b] Jiaoyang Lu,*[a] and Juyoung Yoon*[b, c]

Acute lung injury (ALI) is a severe respiratory disorder driven by uncontrolled inflammation, where early diagnosis and intervention are critical. Recent evidence implicates Golgi apparatus dysfunction in ALI progression, but its biophysical changes remain unexplored. Here, we report **GV**, a novel Golgi-targeted fluorescent probe with high photostability, low cytotoxicity, and excellent specificity, enabling sensitive imaging of viscosity changes under stress. Using both cellular and mouse models of ALI, we demonstrated a significant increase in Golgi viscosity during disease progression. These findings suggest that Golgi viscosity may serve as a potential biomarker for ALI and establish **GV** as a powerful tool for investigating organelle-level biophysical alterations in inflammatory diseases.

1. Introduction

Acute lung injury (ALI) is a severe and common clinical syndrome, primarily characterized by damage to the capillary endothelium and disruption of the alveolar-capillary barrier, ultimately leading to acute hypoxemic respiratory failure.[1–3] ALI can be triggered by a variety of pulmonary and extrapulmonary insults. Despite its heterogeneous etiology, increasing evidence suggests that an uncontrolled acute inflammatory response is a central pathological mechanism driving its development. ALI remains associated with high incidence and mortality, with fatality rates ranging from 30% to 50%.[4,5] Even among survivors, long-term quality of life is often significantly impaired, imposing a considerable medical and economic burden on patients and society. Therefore, the ability to visualize and accurately assess inflammatory processes is critical to understanding the mechanisms underlying ALI onset and progression.

Viscosity is a fundamental biophysical property of the cellular microenvironment, essential for maintaining homeostasis and supporting normal physiological functions. It plays a crucial role in key biological processes such as membrane fusion, protein folding and conformational transitions, and peptide aggregation.[6–8] Emerging evidence indicates that dysregulated intracellular viscosity is closely associated with various metabolic and inflammatory diseases, including inflammation, ALI, nonalcoholic fatty liver disease (NAFLD), and certain cancers.[9,10] Moreover, the viscosity of many organelles increases during inflammatory pathological states.[11–14] These findings highlight the urgent need for precise, real-time monitoring of viscosity dynamics in living systems, which is crucial for elucidating disease-related biophysical changes and developing responsive molecular imaging tools and therapeutic strategies.

However, accurately detecting viscosity in complex pathological conditions like ALI remains technically challenging, primarily due to the highly dynamic and intricate nature of the in vivo microenvironment.[15–18] Against this backdrop, the Golgi apparatus has emerged as a promising research focus. As a central trafficking hub of the endomembrane system, the Golgi is responsible for processing, sorting, and transporting newly synthesized and recycled proteins and lipids to their correct subcellular destinations. Dysfunction of the Golgi can disrupt macromolecular trafficking and cause abnormal accumulation, potentially altering its local physicochemical properties—particularly viscosity.[19,20] We therefore hypothesize that Golgi-specific viscosity changes not only reflect disturbances in its functional state but may also serve as a sensitive biophysical indicator of early stress responses in ALI. Nevertheless, no direct experimental evidence currently links Golgi viscosity to ALI progression, largely because of the lack of molecular probes or imaging tools capable of in situ visualization of viscosity at the sub-organelle level under physiological conditions.

[a] Y. Li, Z. Yang, J. Lei, Q. Dai, G. Li, J. Lu
Hunan Key Laboratory of the Research and Development of Novel Pharmaceutical Preparations, Hunan Provincial University Key Laboratory of the Fundamental and Clinical Research on Functional Nucleic Acid, The First Clinical College of Changsha Medical University, Changsha 410219, P. R. China
E-mail: joyerlu@qq.com

[b] H. Xu, J. Yoon
Department of Chemistry and Nanoscience, Ewha Womans University, Seoul 03760, Republic of Korea
E-mail: xuhai@my.swjtu.edu.cn
jyoon@ewha.ac.kr

[c] J. Yoon
Graduate Program in Innovative Biomaterials Convergence, Ewha Womans University, Seoul 03760, Republic of Korea

Supporting information for this article is available on the WWW under https://doi.org/10.1002/chem.202502835

© 2025 The Author(s). Chemistry – A European Journal published by Wiley-VCH GmbH. This is an open access article under the terms of the Creative Commons Attribution-NonCommercial License, which permits use, distribution and reproduction in any medium, provided the original work is properly cited and is not used for commercial purposes.

© 2025 The Author(s). Chemistry – A European Journal published by Wiley-VCH GmbH

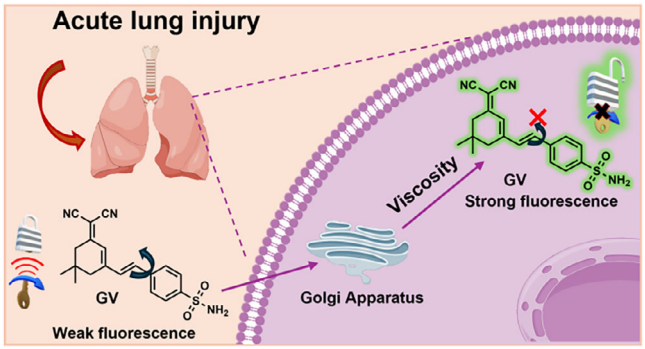


Figure 1. Design and application concept of Golgi specific fluorescent probe **GV** for ALI.

Fluorescent molecular probes, owing to their tunable chemical structures, high spatiotemporal resolution, and noninvasive imaging capabilities, have become indispensable tools for studying dynamic biological processes in living systems.[21–26] In recent years, various viscosity-responsive probes have been developed and successfully applied in live-cell and in vivo imaging.[27–30] However, most of these probes lack organelle specificity, limiting their ability to accurately measure viscosity at the subcellular level.[31–33] To address this limitation, organelle-targeted viscosity probes for mitochondria, lysosomes, and the endoplasmic reticulum have been reported.[34–38] Nonetheless, probes specifically designed for Golgi-localized viscosity sensing remain extremely limited. Although a few viscosity-sensitive probes with Golgi-targeting capability have been described, none have been explicitly developed to monitor viscosity changes under stress conditions associated with ALI.[25–41] This gap underscores the urgent need for novel Golgi-targeted viscosity probes capable of real-time, dynamic monitoring of subcellular biophysical changes during ALI progression.

In this study, we report a structurally simple and readily synthesized fluorescent probe (**GV**) for the sensitive detection of Golgi viscosity (Figure 1). **GV** exhibits excellent Golgi-targeting specificity, reliable viscosity responsiveness, and low cytotoxicity, enabling real-time imaging of Golgi viscosity changes under pathophysiological conditions. Notably, this work presents in situ fluorescence imaging evidence of elevated Golgi viscosity in lung tissues from ALI mouse models. This breakthrough not only establishes a direct correlation between Golgi viscosity and ALI progression, but also highlights its potential as a novel diagnostic biomarker. Collectively, our findings demonstrate that **GV** provides a powerful platform for probing subcellular biophysical alterations and opens new avenues for the investigation and clinical evaluation of ALI and other viscosity-related diseases.

2. Results and Discussion

2.1. Materials and Instruments

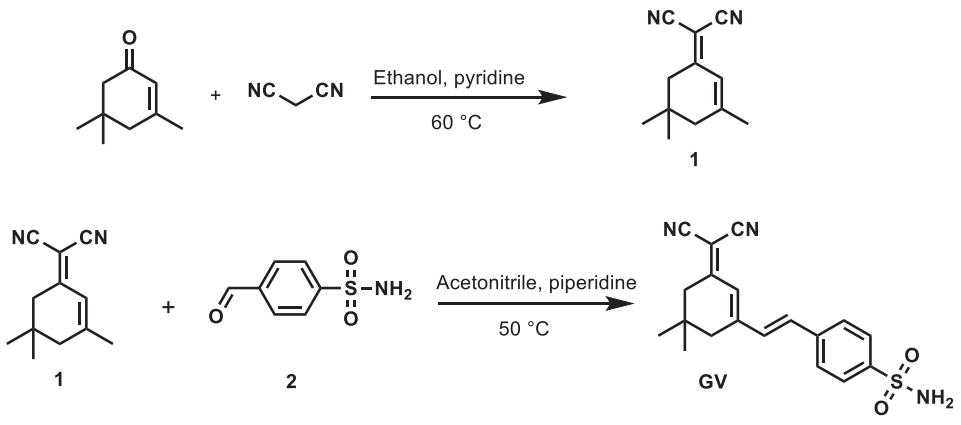
All chemical reagents used in this study were purchased from commercial suppliers and used without further purification. The commercially available fluorescent tracker was obtained from Beyotime Biotechnology.

^{1}H and ^{13}C nuclear magnetic resonance (NMR) spectra were recorded on a Bruker NMR spectrometer. High-resolution mass spectrometry (HRMS) data were acquired using a Bruker Maxis ultra-high-resolution time-of-flight (UHR-TOF) mass spectrometer. Fluorescence emission spectra were collected using an Edinburgh Instruments FLS-920 spectrofluorometer. Cellular fluorescence imaging was performed on a Carl Zeiss LSM900 confocal laser scanning microscope. Fluorescence imaging of tissue sections was performed using the 3DHISTECH Pannoramic MIDI digital pathology scanning and analysis system.

2.2. Synthesis Procedures

The synthetic route of probe **GV** was shown in Scheme 1. Structural identification of **GV** was confirmed by ^{1}H, ^{13}C NMR and HR-MS spectrometry (Figures S1-S3).

Synthesis of compound 1. Compound 1 was synthesized following a previously reported method as described in the literature.[42] Maleimide (0.33 g, 5 mmol) and isophorone (0.75 mL, 5 mmol) were added to a 25 mL two-necked round-bottom flask, followed by the addition of 10 mL anhydrous ethanol as the reaction solvent. A catalytic amount of pyridine was added dropwise. The reaction mixture was stirred at 60 °C



Scheme 1. Synthetic Route for **GV**.

© 2025 The Author(s). Chemistry – A European Journal published by Wiley-VCH GmbH

15213765, 2025, 70, Downloaded from https://chemistry-europe.onlinelibrary.wiley.com/doi/10.1002/chem.202502835 by Ewha Womans University Library, Wiley Online Library on [27/05/2026]. See the Terms and Conditions (https://onlinelibrary.wiley.com/terms-and-conditions) on Wiley Online Library for rules of use; OA articles are governed by the applicable Creative Commons License

for 8 hours. After completion, the mixture was cooled to room temperature and poured into 100 mL of ice water. The flask was sealed and stored at 4 °C overnight. The resulting gray solid was collected by vacuum filtration and dried under reduced pressure to afford compound 1 (0.67 g, yield: 72%).

Synthesis of **GV**. Compound 1 (1.5 g, 8 mmol) and compound 2 (4-formylbenzenesulfonamide, 1.86 g, 8 mmol) were dissolved in 10 mL of anhydrous acetonitrile under an argon atmosphere. To this solution, 0.5 mL of piperidine was added as a catalyst. The reaction mixture was stirred at 50 °C under argon overnight. Upon completion, the reaction mixture was cooled to room temperature, and the solvent was removed under reduced pressure. The crude product was purified by silica gel column chromatography to afford the final product **GV** as a yellow solid (1.76 g, yield: 55%). ^{1}H NMR (500 MHz, DMSO-d_6) δ = 7.81 (dt, J = 22.4, 8.4 Hz, 4H), 7.50 (d, J = 16.2 Hz, 1H), 7.39 (s, 2H), 7.28 (d, J = 16.2 Hz, 1H), 6.89 (s, 1H), 2.57 (s, 2H), 2.44 (s, 2H), 0.96 (s, 7H). ^{13}C NMR (126 MHz, DMSO) δ = 170.33, 155.14, 144.16, 139.23, 135.57, 132.00, 128.20, 128.04, 126.19, 123.97, 113.72, 112.90, 77.45, 61.14, 42.29, 38.11, 31.73, 27.46, 25.30. HR-MS (Figure S3) *m/z* calcd for $C_{19}H_{19}N_3O_2S$ [M + H^+]: 352.1120, found 352.1111.

2.3. Spectroscopic Measurements

The stock solution of the fluorescent probe **GV** was first prepared by dissolving the compound in an appropriate DMSO solvent, followed by dilution to a final concentration of 10 μM for spectroscopic analysis. All interfering substances were freshly prepared in deionized water to ensure consistency across measurements. Fluorescence spectra were acquired using the fluorescence spectrophotometer. The excitation wavelength was set at 390 nm, with both excitation and emission slit widths maintained at 5.0 nm to optimize resolution and signal intensity.

2.4. Cell Culture and Fluorescence Imaging

Human alveolar epithelial A549 cells, obtained from Xiangya School of Medicine, Central South University (Changsha, China), were cultured in Dulbecco's Modified Eagle Medium (DMEM) supplemented with 10% fetal bovine serum (FBS). Cells were maintained in a humidified incubator at 37 °C with 5% CO_2 and 95% air. For imaging experiments, cells were seeded into 35 mm glass-bottom culture dishes and incubated for 24 hours to ensure adequate adhesion and formation of a monolayer. Prior to staining, cells were washed three times with phosphate-buffered saline (PBS, pH 7.4) and kept at 37 °C to maintain physiological conditions. Confocal laser scanning microscopy was used to acquire fluorescence images.

2.5. In Vivo Viscosity Imaging in Mice

BALB/c mice were purchased from SJA Laboratory Animal Co., Ltd. (Changsha, China) and maintained under standard housing conditions throughout the experimental period. All animal procedures complied with national regulations and were approved by the Institutional Animal Care and Use Committee of Changsha Medical University.

To establish a lipopolysaccharide (LPS)-induced ALI model, mice were intraperitoneally injected with LPS at a dose of 10 mg/kg, followed by observation for 6 hours. For fluorescence imaging of lung tissues, cryosections approximately 10 μm thick were prepared and incubated with the fluorescent probe **GV** (50 μM) at 37 °C for 1 hour. Fluorescence signals were then acquired using a fluorescence microscope.

3. Results and Discussion

3.1. Spectroscopic Response of GV to Viscosity

To assess the viscosity sensitivity of **GV**, its photophysical behavior under varying viscosity conditions was systematically investigated. First, the UV-visible absorption spectra of **GV** were recorded in both low- and high-viscosity environments. As shown in Figure 2A, **GV** exhibited a characteristic absorption peak centered at 380 nm in PBS. In contrast, in 90% glycerol, the UV absorption intensity increased markedly, likely due to restricted intramolecular rotation. Next, the fluorescence spectra of **GV** were measured in glycerol-PBS mixtures with different viscosities (Figure 2B, Table S1). At low viscosity, **GV** displayed relatively weak fluorescence emission. As the viscosity increased, the fluorescence intensity at 510 nm progressively intensified, exhibiting a strong linear correlation between log(F_{510}) and log(viscosity), with a correlation coefficient of R^2 = 0.992 (Figure 2C). This relationship is described by the equation $\log(F_{510}) = 2.5438 + 0.4517 \log \eta$, demonstrating that **GV** is highly sensitive to microenvironmental viscosity changes.

In complex biological environments, good selectivity and anti-interference are essential requirements for viscosity probes. To this end, the fluorescence response of **GV** was first evaluated across a wide pH range. As shown in Figure S4, **GV** maintained stable fluorescence intensity in solutions ranging from pH 4.0 to 11.0, indicating that physiological pH fluctuations had little effect on its performance, thereby supporting its applicability in biological systems. To assess potential interference, **GV** was exposed to common biological species, including representative cations (Al^{3+}, Cu^{2+}, Ca^{2+}, K^+, Mg^{2+}, Na^+, Zn^{2+}), anions (Br^-, Cl^-, HCO_3^-, I^-, NO_3^-, PO_4^{3-}, SO_4^{2-}), and biothiols (homocysteine, glutathione, cysteine, H_2S) (Figure 2D). Among these, only glycerol significantly enhanced the fluorescence intensity of **GV**, while all other analytes had negligible effects, confirming the excellent selectivity of **GV** for viscosity. Further competition experiments were performed to determine whether these analytes interfered with **GV**'s fluorescence response. As shown in Figure S5, **GV** maintained consistent fluorescence intensity in the presence of all tested substances, further validating its high specificity for viscosity. Furthermore, the fluorescence response of **GV** was systematically examined in solvents of varying polarity and in aqueous mixtures with different water fractions (Figure S6). The results demonstrated that significant

© 2025 The Author(s). Chemistry – A European Journal published by Wiley-VCH GmbH

15213765, 2025, 70, Downloaded from https://chemistry-europe.onlinelibrary.wiley.com/doi/10.1002/chem.202502835 by Ewha Womans University Library, Wiley Online Library on [27/05/2026]. See the Terms and Conditions (https://onlinelibrary.wiley.com/terms-and-conditions) on Wiley Online Library for rules of use; OA articles are governed by the applicable Creative Commons License

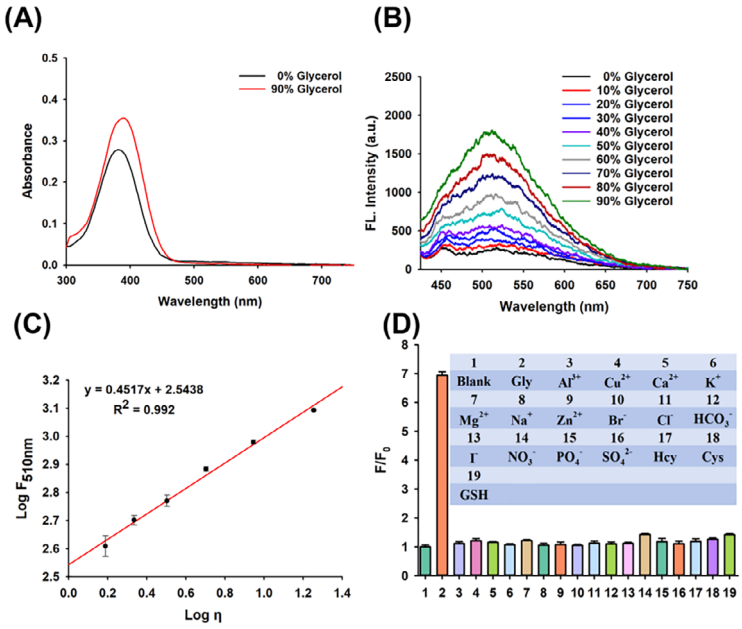


Figure 2. a) UV–Vis absorption spectra of **GV** (10 μM) recorded in phosphate-buffered saline (PBS) and 90% glycerol solution. b) Fluorescence emission spectra of **GV** in PBS/glycerol mixtures with varying viscosities. c) Linear correlation between the logarithm of fluorescence intensity at 510 nm and the logarithm of medium viscosity. d) Relative fluorescence intensities of **GV** (10 μM) in the presence of various potential interfering species (100 μM). The excitation wavelength was set to 390 nm.

fluorescence enhancement occurred only under high-viscosity conditions. In addition, the photostability of **GV** was evaluated in both water and 90% glycerol over 60 minutes (Figure S7). The fluorescence signal remained stable throughout the observation period, demonstrating that **GV** possesses good photostability, making it suitable for long-term imaging applications.

To gain deeper insight into the viscosity-sensing mechanism of **GV**, we carried out density functional theory (DFT) calculations. As shown in Figure S8, the energy gap of **GV** in its planar excited-state conformation is calculated to be 3.321 eV. In this planar configuration, the HOMO electrons are delocalized across the entire molecule, while the LUMO electrons are primarily localized on the strongly electron-withdrawing malononitrile moiety. Upon molecular rotation, the HOMO electrons become localized and no longer span the entire molecule, thereby disrupting the intramolecular charge transfer (ICT) process. These findings indicate that, in the excited state, strong charge transfer occurs from the dimethylaniline donor to the triphenyl phosphate acceptor groups, leading to a typical torsional ICT (TICT) process. The increase in environmental viscosity effectively restricts molecular torsion, thereby suppressing the TICT process and enhancing fluorescence emission.

3.2. Visualization of Viscosity in Live Cells

Given the strong spectral response of **GV** to viscosity under in vitro conditions, we further explored its utility in monitoring intracellular viscosity changes in living cells and biological systems. The cytotoxicity of **GV** was first assessed using a standard MTT assay (Figure S9). The results showed that **GV** exhibited negligible toxicity toward A549 cells within the tested concentration range, confirming its excellent biocompatibility and suitability for live-cell imaging applications.

To verify the Golgi-targeting capability of **GV**, we performed colocalization experiments to determine its intracellular localization. A549 cells were co-stained with **GV** and the commercial Golgi marker dye, Golgi Track Red. As shown in Figure 3, the fluorescence of **GV** exhibited a strong overlap with Golgi-Tracker Red, yielding a Pearson's correlation coefficient of 0.93, which confirms its excellent Golgi-targeting capability. Meanwhile, the colocalization coefficient between **GV** and Mito-Tracker Red exceeded 0.6, suggesting that the probe can also partially localize to mitochondria. However, the substantially higher overlap with Golgi-Tracker Red indicates that GV possesses much stronger specificity toward the Golgi apparatus.

Owing to its excellent optical properties and low cytotoxicity, **GV** was further applied to imaging Golgi viscosity changes in A549 cells under stress conditions. Nystatin, a well-known ionophore, has been reported to disrupt ion homeostasis and induce changes in intracellular viscosity.[43] As shown in Figure 4A, cells treated with **GV** alone exhibited weak fluorescence signals, whereas cells co-incubated with nystatin displayed markedly enhanced fluorescence intensity. Quantitative analysis using Image J (Figure 4B) revealed that the fluorescence intensity in the nystatin-treated group increased by approximately twofold compared to the control group. These findings confirm that **GV** can effectively respond to intracellular viscosity changes and visualize nystatin-induced microenvironmental alterations, highlighting its potential as a powerful fluorescent probe for real-time monitoring of cellular viscosity dynamics.

Monensin is widely recognized as a potent inducer of oxidative stress, particularly noted for disrupting Golgi function by impairing the activity of Golgi-resident proteins through

© 2025 The Author(s). Chemistry – A European Journal published by Wiley-VCH GmbH

15213765, 2025, 70, Downloaded from https://chemistry-europe.onlinelibrary.wiley.com/doi/10.1002/chem.202502835 by Ewha Womans University Library, Wiley Online Library on [27/05/2026]. See the Terms and Conditions (https://onlinelibrary.wiley.com/terms-and-conditions) on Wiley Online Library for rules of use; OA articles are governed by the applicable Creative Commons License

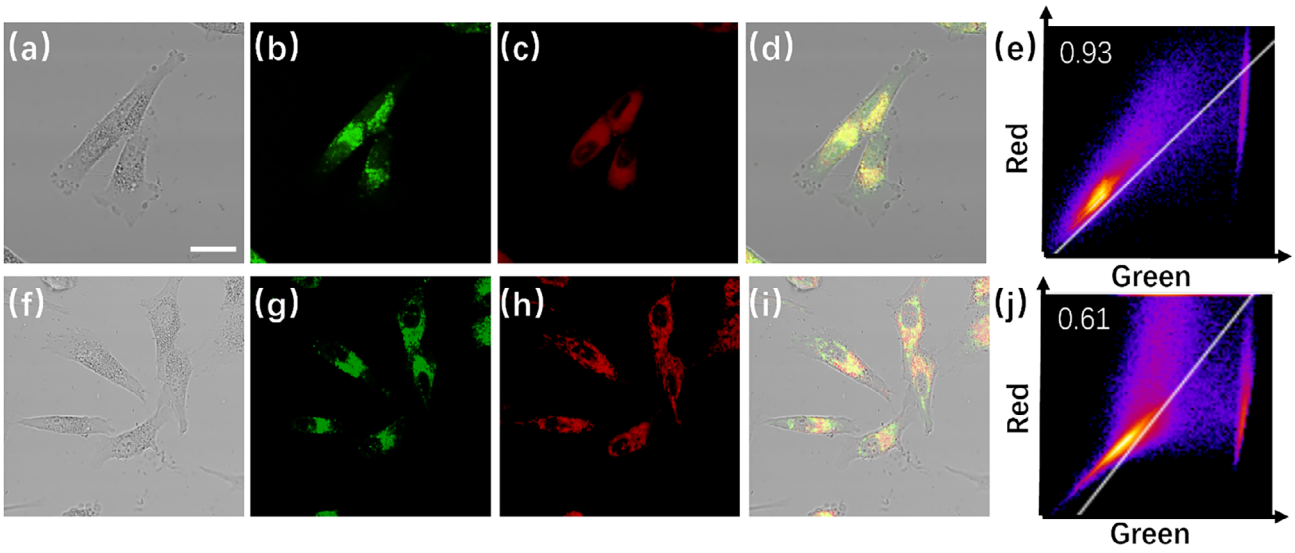


Figure 3. Colocalization analysis of **GV** in A549 cells. a, f) Bright-field image. b, g) Fluorescence image of **GV** (10 μM) after treatment with nystatin (10 μM) in the green channel (excitation at 405 nm, emission collected at 480–560 nm). Fluorescence image of c) Golgi-Tracker Red or h) Mito-Tracker Red in the red channel (1 μM; excitation at 633 nm, emission window: 640–690 nm). d, i) Merged image. e, j) Fluorescence intensity correlation scatter plot. Scale bar: 10 μm.

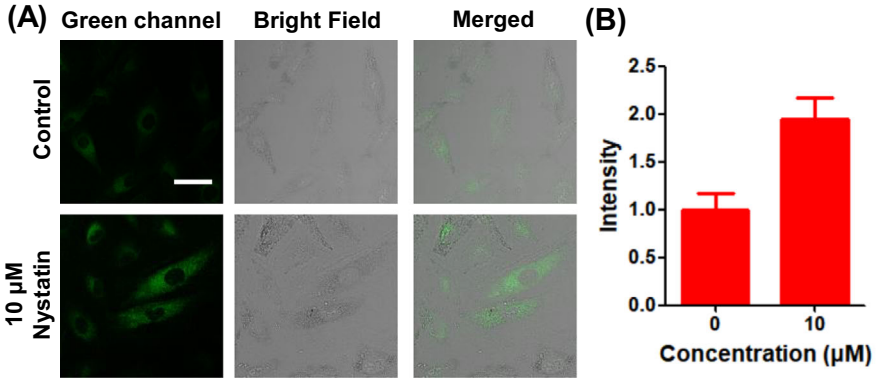


Figure 4. a) Confocal imaging of **GV** in A549 cells before and after treatment with nystatin. b) Fluorescence intensity in (A) Scale bar: 10 μm. Excitation: 405 nm; Emission: 480–560 nm.

redox imbalance.[44] In this study, the fluorescent probe **GV** was employed to visualize changes in Golgi viscosity during monensin-induced oxidative stress. A549 cells were divided into four groups: one control group incubated with **GV** (10 μM) for 30 minutes under normal conditions, and three experimental groups pretreated with increasing concentrations of monensin (10 μM, 20 μM, and 50 μM) for 24 hours to induce varying levels of oxidative stress in the Golgi. After monensin treatment, cells were incubated with **GV** (10 μM) for an additional 30 minutes before imaging (Figure 5). As expected, the control group exhibited the weakest fluorescence, whereas monensin-treated cells showed progressively stronger fluorescence signals, which positively correlated with monensin concentration. These results demonstrate that **GV** can sensitively detect changes in Golgi viscosity under oxidative stress in a concentration-dependent manner.

Collectively, these findings underscore the potential of **GV** as a Golgi-targeted fluorescent probe for monitoring microenvironmental changes during oxidative stress, providing a valuable tool for investigating the molecular mechanisms of Golgi-associated oxidative stress in various disease contexts.

A549 cells were exposed to LPS for 24 hours to establish an in vitro ALI model, as previously described.[35] Following LPS induction, the cells were incubated with the fluorescent probe **GV** for 30 minutes and then imaged (Figure 6A,). Compared with the control group treated with **GV** alone, LPS-stimulated cells exhibited markedly enhanced green fluorescence, indicating an increase in intracellular viscosity under inflammatory stress. Flow cytometric analysis further confirmed that the fluorescence intensity in the LPS-treated group was significantly higher than in the control group (Figure 6B), consistent with the fluorescence microscopy observations. Additionally, flow cytometry was used to assess LPS-induced apoptosis. After 24 hours of LPS treatment at a concentration of 2.5 μg/mL, the apoptosis rate reached 9.75%, significantly higher than that of the control group (3.34%) (Figure 6D, E). These results collectively highlight the increase in intracellular viscosity associated with LPS-induced apoptosis under inflammatory stress.

© 2025 The Author(s). Chemistry – A European Journal published by Wiley-VCH GmbH

15213765, 2025, 70, Downloaded from https://chemistry-europe.onlinelibrary.wiley.com/doi/10.1002/chem.202502835 by Ewha Womans University Library, Wiley Online Library on [27/05/2026]. See the Terms and Conditions (https://onlinelibrary.wiley.com/terms-and-conditions) on Wiley Online Library for rules of use; OA articles are governed by the applicable Creative Commons License

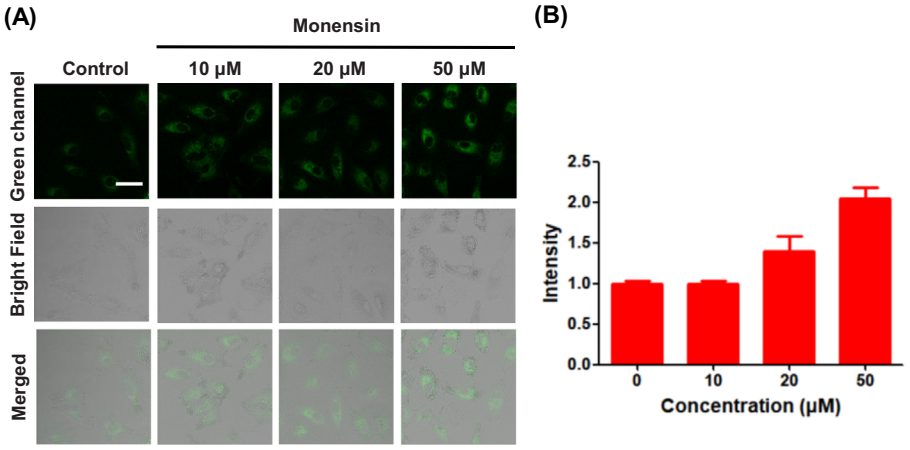


Figure 5. a) Fluorescence imaging of A549 cells incubated with **GV** (10 μM) alone or cotreated with increasing concentrations of monensin (10 μM, 20 μM, and 50 μM) for 24 hours, followed by **GV** staining. b) Quantitative analysis of fluorescence intensity corresponding to the images shown in (A). Scale bar: 10 μm. Excitation: 405 nm; Emission: 480–560 nm.

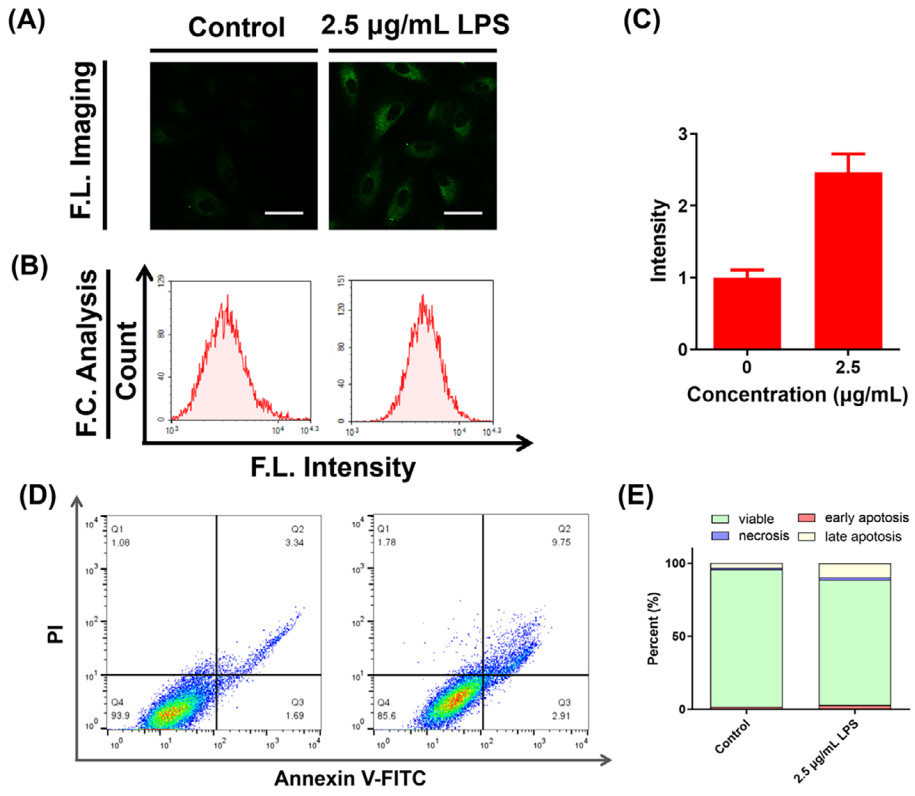


Figure 6. Visualization of viscosity fluctuations in the ALI cellular model using **GV**. a) Fluorescence imaging of A549 cells incubated with **GV** (10 μM) as a control, and after stimulation with LPS (2.5 μg/mL, 24 hours) to induce the ALI model. b) Flow cytometric analysis of intracellular fluorescence signal corresponding to the conditions shown in (A). c) Quantification of fluorescence intensity from images in (A). Scale bar: 10 μm. Excitation wavelength: 405 nm; emission range: 480–560 nm. d) Flow cytometric analysis of A549 cells stained with Annexin V-FITC and PI. Cells are categorized into four populations based on fluorescence: viable (Annexin V^-/PI^-), early apoptotic (Annexin V^+/PI^-), late apoptotic (Annexin V^+/PI^+), and necrotic (Annexin V^-/PI^+). The percentages in each quadrant represent the proportion of cells in each state. e) Quantitative analysis of the distribution of A549 cells among the different states identified in Panel (D).

3.3. Visualization of Viscosity in Vivo

To assess the applicability of **GV** in the context of ALI, we evaluated its performance in a well-established murine ALI model induced by LPS, which is widely recognized for recapitulating key pathological features of the disease.[45] Following intraperitoneal injection of LPS to induce ALI, mouse lung tissues were excised, incubated ex vivo with the **GV** probe, and imaged using a small-animal imaging system (Figure 7A,B). As shown in Figure 7C,D, a substantial increase in fluorescence intensity was observed in the lungs of LPS-treated mice compared to the control group. These results were further verified by H&E staining. The H&E

© 2025 The Author(s). Chemistry – A European Journal published by Wiley-VCH GmbH

15213765, 2025, 70, Downloaded from https://chemistry-europe.onlinelibrary.wiley.com/doi/10.1002/chem.202502835 by Ewha Womans University Library, Wiley Online Library on [27/05/2026]. See the Terms and Conditions (https://onlinelibrary.wiley.com/terms-and-conditions) on Wiley Online Library for rules of use; OA articles are governed by the applicable Creative Commons License

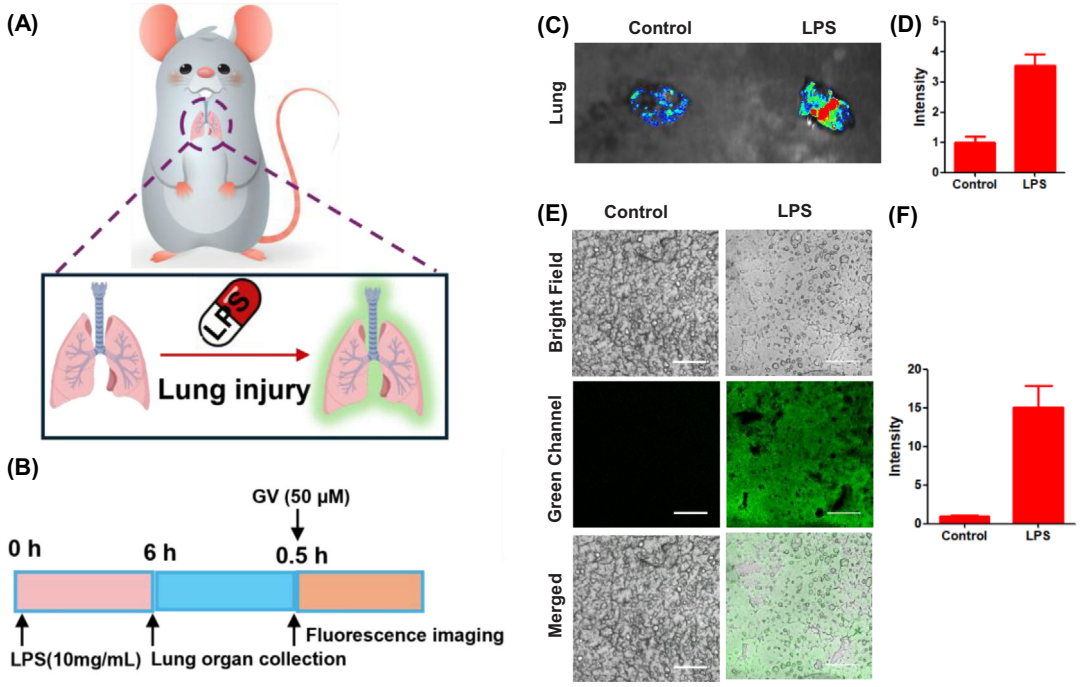


Figure 7. a) Schematic illustration showing the use of **GV** to monitor viscosity changes in a lipopolysaccharide (LPS)-induced ALI model. b) Experimental timeline depicting the procedure for probe administration, tissue collection, and fluorescence imaging analysis. c) Ex vivo fluorescence imaging of whole lungs isolated from control and LPS-treated mice. d) Quantitative comparison of fluorescence intensity between the control and LPS groups based on panel (C). e) Fluorescence microscopy images of lung tissue sections from both groups. Scale bar: 100 μm. (f) Quantified fluorescence intensity of the tissue sections shown in panel (E).

staining results confirmed the successful establishment of the ALI model, as evident from the distinct pathological differences between the control and model groups (Figure S10). To further corroborate these findings, frozen lung tissue sections were prepared and imaged. Consistent with the whole-organ imaging results, enhanced fluorescence signals were also detected in tissue slices from LPS-treated mice (Figure 7E, F), confirming the robustness and reliability of **GV** for ex vivo pulmonary imaging. Collectively, these results demonstrate that lung tissue viscosity progressively increases during the progression of ALI, and that **GV** is an effective molecular tool for visualizing these changes. This highlights its potential utility for probing the pathophysiological mechanisms of ALI and other inflammation-related diseases.

4. Conclusion

In summary, we have developed **GV**, a novel Golgi-targeted fluorescent probe that combines high sensitivity to microenvironmental viscosity changes, excellent organelle specificity, and minimal cytotoxicity. Through systematic in vitro and in vivo experiments, we demonstrated that **GV** enables real-time visualization of Golgi viscosity dynamics, particularly under oxidative and inflammatory stress conditions associated with ALI. Notably, this study provides in situ fluorescence imaging evidence of increased Golgi viscosity in the lung tissue of ALI mice, revealing a previously unrecognized link between subcellular biophysical alterations and disease progression. By addressing the current lack of molecular tools for organelle-specific viscosity sensing, **GV** offers a powerful platform for investigating the pathophysiological role of viscosity changes in ALI and related diseases.

Supporting Information

The authors have cited additional references within the Supporting Information.

Acknowledgments

The authors are grateful for financial support from the National Natural Science Foundation of China (No. 32201108), the Science and Technology Innovation Program of Hunan Province (No. 2022RC1167), the Natural Science Foundation of Hunan Province (No. 2025JJ60753, 2024JJ5053, 2022JJ40529, 2023JJ40084), the Scientific Research Fund of Hunan Provincial Education Department (No. 24B0891, 24B0893, 22C0672, 23C0447, 23B0883). J. Yoon thanks to the Nano & Material Technology Development Program through the National Research Foundation of Korea (NRF) funded by Ministry of Science and ICT (RS-2024-00407093) and the National Research Foundation of Korea (NRF) grant funded by the Korea government (MSIT) (RS-2023-00217701).

© 2025 The Author(s). Chemistry – A European Journal published by Wiley-VCH GmbH

15213765, 2025, 70, Downloaded from https://chemistry-europe.onlinelibrary.wiley.com/doi/10.1002/chem.202502835 by Ewha Womans University Library, Wiley Online Library on [27/05/2026]. See the Terms and Conditions (https://onlinelibrary.wiley.com/terms-and-conditions) on Wiley Online Library for rules of use; OA articles are governed by the applicable Creative Commons License

Conflict of Interest

The authors declare no conflict of interest.

Data Availability Statement

The data that support the findings of this study are available from the corresponding author upon reasonable request.

Keywords: Acute lung injury · Fluorescent probe · Golgi targeted · Viscosity

[1] E. H. Lee, M. H. Shin, M. Gi, J. Park, D. Song, Y. M. Hyun, J. H. Ryu, J. K. Seong, Y. Jeon, G. Han, W. Namkung, M. S. Park, J. Y. Choi, *Theranostics* **2020**, *10*, 9913.
[2] R. Su, H. Wang, C. Xiao, Y. Tao, M. Li, Z. Chen, *Biomater. Sci.* **2021**, *9*, 4746.
[3] Y. Cui, X. Wang, F. Lin, W. Li, Y. Zhao, F. Zhu, H. Yang, M. Rao, Y. Li, H. Liang, M. Dai, B. Liu, L. Chen, D. Han, R. Lu, W. Peng, Y. Zhang, C. Song, Y. Luo, P. Pan, *Aging. Dis.* **2022**, *13*, 899.
[4] E. Fan, D. Brodie, A. S. Slutsky, *JAMA, J. Am. Med. Assoc.* **2018**, *319*, 698.
[5] E. R. Johnson, M. A. Matthay, J. Aerosol, *Med. Pulm. D.* **2010**, *23*, 243.
[6] D. M. Toraldo, F. Peverini, M. De Benedetto, F. De Nuccio, *Lung* **2013**, *191*, 1.
[7] H. Li, Y. Liu, X. Li, X. Li, H. Ma, *Spectrochim Acta A Mol. Biomol. Spectrosc.* **2021**, *246*, 119059.
[8] C. Ma, W. Sun, L. Xu, Y. Qian, J. Dai, G. Zhong, B. Shen, *J. Mater. Chem. B* **2020**, *8*, 9642.
[9] Q. Chen, X. F. Zhang, T. Wang, X. Q. Cao, S. L. Shen, *Anal. Chim. Acta.* **2022**, *1231*, 340443.
[10] M. M. Smith, P. C. Chen, C. S. Li, S. Ramanujam, A. T. Cheung, *Clin. Hemorheol. Microcirc.* **2009**, *41*, 229.
[11] Q. Li, Z. Zheng, Y. Chen, Z. Li, S. Feng, G. Feng, *Anal. Chem.* **2025**, *97*, 1627.
[12] Z. Zheng, S. Feng, S. Gong, X. Tan, G. Feng, *Sens. Actuators, B* **2025**, *442*, 138082.
[13] Z. Li, Q. Li, Y. Liu, Y. Chen, J. Zhang, H. Zhang, G. Feng, *Anal. Chem.* **2025**, *97*, 19186.
[14] X. Tan, J. Hong, S. Jiang, S. Zhang, Y. Chen, G. Feng, *Anal. Chem.* **2024**, *96*, 14860.
[15] Y. Wang, J. Li, Q. Xiang, L. Tang, *Exp. Ther. Med.* **2023**, *25*, 251.
[16] Y. Chen, L. Chen, Q. Zhou, *Herz.* **2021**, *46*, 253.
[17] Y. Liu, H. Li, X. Wang, J. Huang, D. Zhao, Y. Tan, Z. Zhang, Z. Zhang, L. Zhu, B. Wu, Z. Chen, W. Peng, *J. Transl. Med.* **2023**, *21*, 277.
[18] H. Li, Y. Tan, X. Cheng, Z. Zhang, J. Huang, S. Hui, L. Zhu, Y. Liu, D. Zhao,Z. Liu, W. Peng, *Front. Pharmy.* **2022**, *13*, 990307.
[19] D. B. Vlad, D. I. Dumitrascu, A. L. Dumitrascu, *Cells* **2023**, *12*, 1499.
[20] K. M. Galenkamp, C. Commisso, *Front. Cell Dev. Biol.* **2021**, *9*, 664295.
[21] Y. Li, Y. Zhou, J. Lei, Q. Lu, X. Qin, Q. Xu, Y. Wang, C. Wu, Z. Yang, B. He, *J. Mol. Struct.* **2023**, *1271*, 134042.
[22] S. Li, P. Wang, M. Ye, K. Yang, D. Cheng, Z. Mao, Z. Liu, *Anal. Chem.* **2023**, *95*, 5133.
[23] S. Xu, K. C. Yan, Z. H. Xu, Y. Wang, T. D. James, *Chem. Soc. Rev.* **2024**, *53*, 7590.
[24] Z. Wu, Y. Guo, W. Jiang, Y. Yang, P. Wei, T. Yi, *Trends Anal. Chem.* **2024**, *170*, 117461.
[25] Y. Li, Y. Zhou, X. Liu, J. Lei, X. Qin, G. Li, Z. Yang, *Spectrochim. Acta. A.* **2023**, *302*, 123102.
[26] S.-S. Zhang, H. Lee, Y. Zhou, J. Yoon, *Coord. Chem. Rev.* **2026**, *549*, 217255.
[27] X. Yang, D. Zhang, Y. Ye, Y. Zhao, *Coord. Chem. Rev.* **2022**, *453*, 214336.
[28] Y. Li, Z. Zhou, S. Chen, X. Pang, C. Wu, H. Li, Y. Zhang, *Anal. Chim. Acta.* **2023**, *1250*, 340967.
[29] Y. Li, J. Lei, X. Qin, G. Li, Q. Zhou, Z. Yang, *Bioorg. Chem.* **2023**, *138*, 106603.
[30] S. Zeng, C. Chen, Z. Guo, C. Qin, Y. Wang, X. Liu, X. Li, H. Jeong, Y. Hao, D. Zhou, S. Long, Z. Wu, J. Wang, H. Li, X. Peng, J. Yoon, *Angew. Chem., Int. Ed.* **2025**, *64*, e202513815.
[31] N. Gupta, S. I. Reja, V. Bhalla, M. Gupta, G. Kaur, M. Kumar, *J. Mater. Chem. B* **2016**, *4*, 1968.
[32] M. Ren, B. Deng, X. Kong, K. Zhou, K. Liu, G. Xu, W. Lin, *Chem. Commun.* **2016**, *52*, 6415.
[33] Y. Ma, M. Li, H. Sun, J. Y. Ge, Y. Bai, L. Qiu, Z. Chen, *Chem. Commun.* **2023**, *59*, 14025.
[34] H. Song, W. Zhang, Y. Zhang, C. Yin, F. Huo, *Chem. Eng. J.* **2022**, *445*, 136448.
[35] P. Wang, S. Ai, M. Deng, Y. Liu, Y. Liu, L. He, S. Li, *Talanta* **2024**, *278*, 126506.
[36] A. Silswal, A. L. Koner, *Chem. Commun.* **2023**, *59*, 1769.
[37] S. Zeng, Y. Wang, C. Chen, H. Kim, X. Liu, M. Jiang, Y. Yu, Y. S. Kafuti, Q. Chen, J. Wang, X. Peng, H. Li, J. Yoon, *Angew. Chem., Int. Ed.* **2024**, *63*, e202316487.
[38] Y. Lee, B. Hwang, B. Sun, H. Xu, L. Liu, J. Yoon, *Bull. Korean Chem. Soc.* **2025**, *46*, 859.
[39] C. Liu, L. Zhou, Y. Zheng, H. Man, Z. Ye, X. Zhang, Y. Xiao, *Chem. Commun.* **2022**, *58*, 10052.
[40] X. Wang, X. Li, Z. Liu, Y. Meng, X. Fan, H. Wang, B. Xue, *Talanta* **2024**, *278*, 126497.
[41] W. Wu, L. Zhao, Y. Zhang, J. Wei, J. Han, Y. Zhang, Z. Zhao, *Sci. Rep.* **2024**, *14*, 1336.
[42] H. Xu, X. R. Liu, Z. H. Cai, J. Zheng, Y. W. Wang, Y. Peng, *Org. Biomol. Chem.* **2022**, *20*, 4782.
[43] J. J. Chao, H. Zhang, Z. Q. Wang, Q. R. Liu, G. J. Mao, D. H. Chen, C. Y. Li, *Anal. Chim. Acta.* **2023**, *1242*, 340813.
[44] J. Li, J. Tang, X. Yang, P. Xie, J. Liu, D. Zhang, Y. Ye, *Sens. Actuators, B* **2022**, *358*, 131513.
[45] N. He, Y. Wang, Y. Huang, L. Chen, X. Wang, C. Lv, S. Yue, *J. Mater. Chem. B* **2020**, *8*, 9899.

Manuscript received: September 14, 2025
Revised manuscript received: November 4, 2025
Version of record online: November 11, 2025

© 2025 The Author(s). Chemistry – A European Journal published by Wiley-VCH GmbH

15213765, 2025, 70, Downloaded from https://chemistry-europe.onlinelibrary.wiley.com/doi/10.1002/chem.202502835 by Ewha Womans University Library, Wiley Online Library on [27/05/2026]. See the Terms and Conditions (https://onlinelibrary.wiley.com/terms-and-conditions) on Wiley Online Library for rules of use; OA articles are governed by the applicable Creative Commons License